The role of novel imaging in prostate cancer focal therapy: treatment and follow-up

Michael B. Rothberg[a], *Jacob J. Enders*[a], *Zachary Kozel*[a], *Nikhil Gopal*[a], *Baris Turkbey*[b], *and Peter A. Pinto*[a]

Purpose of review
Multiparametric magnetic resonance imaging (mpMRI) has fundamentally changed how intraprostatic lesions are visualized, serving as a highly sensitive means for detecting clinically significant prostate cancer (csPCa) via image-targeted biopsy. However, limitations associated with mpMRI have led to the development of new imaging technologies with the goal of better characterizing intraprostatic disease burden to more accurately guide treatment planning and surveillance for prostate cancer focal therapy. Herein, we review several novel imaging modalities with an emphasis on clinical data reported within the past two years.

Recent findings
7T MRI, artificial intelligence applied to mpMRI, positron emission tomography combined with either computerized tomography or MRI, contrast-enhanced ultrasound, and micro-ultrasound are novel imaging modalities with the potential to further improve intraprostatic lesion localization for applications in focal therapy for prostate cancer. Many of these technologies have demonstrated equivalent or favorable diagnostic accuracy compared to contemporary mpMRI for identifying csPCa and some have even shown improved capabilities to define lesion borders, to provide volumetric estimates of lesions, and to assess the adequacy of focal ablation of planned treatment zones.

Summary
Novel imaging modalities with capabilities to better characterize intraprostatic lesions have the potential to improve accuracy in treatment planning, real-time assessment of the ablation zone, and posttreatment surveillance; however, many of these technologies require further validation to determine their clinical utility.

Keywords
focal therapy, multiparametric magnetic resonance imaging, positron emission tomography, prostate cancer, ultrasound

INTRODUCTION

The diagnosis of prostate cancer has historically relied on systematic transrectal ultrasound (TRUS)-guided biopsy. However, without intra-prostatic tumor imaging and targeted biopsies, the sub-optimal sensitivity and specificity of TRUS-guided prostate biopsy for cancer detection (typically reported between 40 and 50%) created a paradigm whereby clinically significant prostate cancer (csPCa) was commonly underdiagnosed and insignificant cancers were overdiagnosed and subsequently overtreated [1]. The recent widespread adaption of multiparametric magnetic resonance imaging (mpMRI) into the diagnostic pathway for clinically localized prostate cancer has overcome the limitations of conventional TRUS imaging. Indeed, MRI-targeted biopsy has been shown to be superior to systematic TRUS-guided biopsy for the identification of prostate cancer [2–6] and the addition of mpMRI/US fusion-guided biopsy has further optimized the detection of csPCa [7,8]. Further, using 3D printed patient-specific molds of the prostate based on preoperative mpMRI to facilitate one-to-one geometric alignment on wholemount histopathology

[a]Urologic Oncology Branch, Center for Cancer Research, National Cancer Institute and [b]Molecular Imaging Branch, Center for Cancer Research, National Institutes of Health, Bethesda, Maryland, USA

Correspondence to Michael B. Rothberg, MD, Urologic Oncology Branch, National Cancer Institute, National Institutes of Health, 10 Center Drive, Room 1-5940, Bethesda, MD 20892, USA.
Tel: +240 858 3971; e-mail: michael.rothberg@nih.gov

Curr Opin Urol 2022, 32:000–000
DOI:10.1097/MOU.0000000000000986

KEY POINTS

- Limitations associated with mpMRI have led to the development of new imaging technologies with the goal of better characterizing intraprostatic disease burden to more accurately guide treatment planning and surveillance for prostate cancer focal therapy.
- Compared to mpMRI, PSMA-targeted radiotracers combined with computerized tomography or MR imaging may improve index lesion detection, more accurately estimate intraprostatic gross tumor volume, and better predict the presence of adverse pathology.
- Using CEUS for real-time evaluation of tissue microvasculature, focal therapists may be able to intraoperatively determine the adequacy of ablation in planned treatment zones and perform an immediate re-treatment, as needed.
- Compared to mpMRI, microUS has demonstrated similar diagnostic accuracy for detecting csPCa and combining microUS-targeted biopsy to mpMRI-targeted biopsy may add further diagnostic benefit.

following radical prostatectomy, prior work at our institution has shown excellent (>98% positive predictive value) correlation for detection of prostate cancer on mpMRI [9].

Despite significant improvements in intraprostatic lesion visualization and a high sensitivity for identifying csPCa, mpMRI is associated with several limitations. Among these are variable performance reports of the negative predictive value (NPV) of a negative mpMRI for csPCa, which range between 84 and 98% [10,11,12▪,13], and the realization that csPCa may not be properly visualized or characterized on mpMRI. These so-called MRI 'invisible' lesions preclude their targeting at the time of biopsy [10]. Additionally, some reports have suggested mpMRI may underestimate tumor volume [14]. To overcome these challenges, some urologists may perform a saturation biopsy where > 20 cores are obtained to ensure adequate gland sampling and cancer detection; however, such techniques may be associated with prolonged procedure times, increased pain, and increased workflow for interpreting pathologists [15]. Despite its various strengths and weaknesses, mpMRI remains the currently accepted gold standard imaging modality to accurately characterize disease burden and determine whether a patient is a suitable candidate for focal therapy. Recent reports have described several novels and exciting imaging modalities with the potential to further improve intraprostatic lesion localization and optimize the delivery of focal therapy for prostate cancer. A summary of the reported diagnostic accuracies for mpMRI and these novel imaging modalities for the detection of csPCa is provided in Table 1.

MAGNETIC RESONANCE IMAGING

Given the limitations associated with 1.5T and 3T mpMRI for the prostate cancer detection, including limited spatial resolution and image quality, 7T MRI is currently being investigated as a means to improve prostate cancer diagnosis. With more than twice the magnetic field strength of 3T MRI, images generated from 7T scanners demonstrate increased signal to noise ratio compared to 3T MRI [16], resulting in higher spatial resolution and improved anatomic detail for prostate imaging [17]. 7T scanners may also reduce imaging time, with reports of high quality T2W images of the prostate at 3 mm slices obtained with an average acquisition time of approximately one and a half minutes [18]. Several recent studies have compared *ex vivo* 7T MRI of fresh radical prostatectomy specimens to the corresponding histopathology. Durand *et al.* [19] imaged 15 fresh specimens and reported the high-resolution images produced by 7T scanners allowed for visualization of both histologically normal structures in the prostate, such as ducts, blood vessels, and stroma, as well as malignant glands and nests of tumor cells; moreover, postprocessing ductograms further distinguished benign from malignant glands. Likewise, Heidkamp *et al.* [20] performed *ex vivo* 7T MRI on 12 radical prostatectomy specimens and reported accurate localization of index lesions and csPCa (Gleason score > 6) (Fig. 1). Although these early reports show promise, 7T MRI has not yet been tested in human subjects for prostate applications and its utility in the setting of focal therapy for prostate cancer is still to be determined.

Recent enthusiasm has been generated for the application of artificial intelligence (AI), and more specifically deep learning (DL), as a potential means to improve the diagnostic performance of mpMRI for the detection of prostate cancer. DL models rely on algorithms that undergo training via the input of 'ground truth' data to develop multilayered, connected networks that mimic human neuron architecture. Following training, these networks can receive input 'test' data to generate predicted results [21]. DL algorithms have the potential to enhance scan quality, automate lesion or gland segmentation, and decrease inter-reader variability by radiologists [22,23].

DL has been applied to several aspects of prostate MRI [24▪]. In addition to the benefits mentioned above, such algorithms have the potential to detect lesions within the prostate and categorize them according to prostate imaging reporting and data

Table 1. Comparison of imaging modalities for identification of clinically significant prostate cancer

Modality	Study	csPCa Cutoff	Sensitivity	Specificity	PPV	NPV
mpMRI	Ahmed *et al.* [2]	≥ G 3+4	88 (84–91)	45 (39–51)	65 (60–69)	76 (69–82)
	Drost *et al.* [3]	≥ G 3+4	91 (83–95)	37 (29–46)	37 (35–39)	91 (86–94)
	Sathianathen *et al.* [12▪]	≥ G 3+4	NR	NR	NR	91 (88–93)
mpMRI with DL	Schelb *et al.* [27]	≥ G 3+4, PIRADS 3	96 (80–100)	22 (10–39)	NR	NR
		≥ G 3+4, PIRADS 4	88 (70–98)	50 (33–67)	NR	NR
	Zhong *et al.* [30]	≥ G 3+4	63.6[a]	80.0[a]	NR	NR
68-Ga-PSMA PET/CT	Donato *et al.* [37]	≥ G 3+4, vs RP	90.1[a]	97.4[a]	NR	NR
		≥ G 3+4, vs biopsy	94.9[a]	92.8[a]	NR	NR
	Kuten *et al.* [42]	≥ G 3+4	85.7[a]	98.2[a]	96.8[a]	91.5[a]
18-F-DCFPyL PET/CT	Gaur *et al.* [41▪]	All cancer	90.9[a]	NR	NR	NR
		≥ G 3+4	100[a]	NR	NR	NR
	Kuten *et al.* [42]	≥ G 3+4	100[a]	90.9[a]	87.5[a]	100[a]
68-Ga-PSMA PET/MRI	Eiber *et al.* [44]	All cancer	76 (68–92)	97 (90–99)	NR	NR
	Ferraro *et al.* [45]	≥ G 4+3 or cancer core length ≥ 6 mm	96[a]	81[a]	89[a]	93[a]
CEUS	Jung *et al.* [50]	Residual cancer following IRE[b]	76[a]	81[a]	73[a]	83[a]
	Bacchetta *et al.* [51▪▪]	Residual ≥ G 3+4 following HIFU	40 (12–74)	65 (43–84)	33 (16–56)	71 (59–82)
MicroUS	Klotz *et al.* [54]	≥ G 3+4	94[a]	22[a]	44[a]	85[a]

CEUS, contrast-enhanced US; DL, deep learning; mpMRI, multiparametric magnetic resonance imaging; PET, positron emission tomography; PSMA, prostate-specific membrane antigen.
Studies reporting sensitivity, specificity, PPV and NPV of different modalities for detecting csPCa with ground truth of histopathology unless otherwise specified. Results are reported as percentage (95% CI). NR: Not reported. RP: Radical prostatectomy.
[a]No 95% CI reported.
[b]Compared to MRI as reference standard.

system (PI-RADS) classification [24▪]. Several recently developed DL algorithms have proven to be capable of highly accurate index lesion detection and tumor volume segmentation and could potentially further optimize treatment planning for focal therapy [25–29]. Schelb *et al.* [27] developed a DL-based AI algorithm with T2W and diffusion-weighted imaging sequences from 250 patients who underwent 3T prostate MRI, with the histopathologic results of combined targeted and

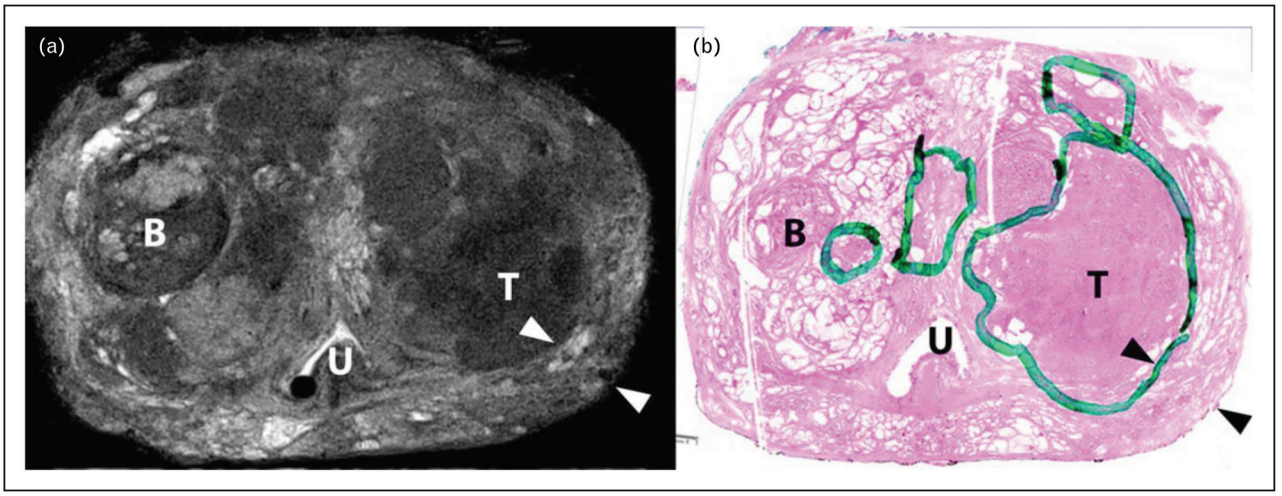

FIGURE 1. (a) *Ex vivo* 7T MRI of a radical prostatectomy specimen demonstrating a lesion in the left transition zone of the prostate (T) with low signal intensity on T2W sequence concerning for prostate cancer, as well as a BPH nodule (B) and the urethra (U); (b) corresponding H&E stained histopathology slide at 100× magnification with pathologist's annotation of a prostate cancer lesion (T). Previously published in: Heidkamp *et al.* [20]. MRI, magnetic resonance imaging; BPH, benign prostatic hyperplasia.

systematic prostate biopsy serving as the ground truth. In the test cohort, they report sensitivities of 96% and 88%, as well as specificities of 22% and 50%, for PI-RADS $\geq$ 3 and $\geq$ 4, respectively, in detecting csPCa (ISUP grade group (GG) $\geq$ 2). Yoo *et al.* [29] defined a training set of 271 patients who underwent 3T prostate MRI with PI-RADS $\geq$ 3 lesions with subsequent prostate biopsy for their DL-based AI model. In the test set, the algorithm demonstrated an AUC of 0.87 (95% CI 0.84 – 0.90) at the slice level and 0.84 (95% CI 0.76–0.91) at the patient level. Additionally, Zhong *et al.* [30] developed a DL-based AI model to both identify and classify intraprostatic lesions as either insignificant or clinically significant (PI-RADS $\geq$ 4) based on 110 patients who underwent 3T mpMRI with corresponding whole-mount histopathology available. In the test set, the algorithm demonstrated an AUC of 0.73 (95% CI 0.58 – 0.88) for classifying PI-RADS $\geq$ 4 lesions. Although AI algorithms show great promise to detect suspicious lesions and characterize the presence of csPCa, further refinement of these models with larger and more diverse data sets is required prior to clinical adaption.

POSITRON EMISSION TOMOGRAPHY

To overcome the shortcomings of mpMRI, there has been growing interest in the use of positron emission tomography (PET) imaging to better characterize prostate cancer biology and the extent of intraprostatic lesions for potential applications in focal therapy treatment and postablation surveillance. Previous investigations have reported the utility of PET imaging for staging in the setting of localized, high-risk disease, biochemical recurrence, or metastatic prostate cancer; however, the clinical utility of individual PET tracers varies widely. Although tracers such as ^{18}F-FDG (^{18}F-fluorodeoxyglucose), ^{18}F-NaF, ^{11}C-choline, and ^{18}F-fluciclovine may be able to identify locoregional or metastatic disease, they are generally limited by either poor sensitivities or specificities for the initial detection of prostate cancer, as well as an inability to accurately define the boundaries and volumes of intraprostatic lesions [31]. More recent investigations have evaluated PET tracers targeting prostate-specific membrane antigen (PSMA), a transmembrane protein upregulated in most csPCa [32], in the setting of localized, high-risk disease and biochemical recurrence [33–36].

Several PSMA-targeting radiotracers, notably ^{68}Ga-PSMA-11, ^{18}F-DCFPyL ((2*S*)-2-[[(1*S*)-1-carboxy-5-[(6-(^{18}F)fluoranylpyridine-3-carbonyl)amino]pentyl]carbamoylamino]pentanedioic acid), and ^{18}F-PSMA-1007, are currently being evaluated for their ability to characterize intraprostatic tumors. Donato *et al.* [37] recently compared ^{68}Ga-PSMA-11 PET/CT and mpMRI to histopathology in 144 patients (prostate biopsy in all patients, radical prostatectomy specimen in a subset). Despite similar sensitivities for index lesion detection between ^{68}Ga-PSMA-11 PET/CT and mpMRI (90.1% and 83.1%, respectively) and high concordance rates (80.1% for index lesions, 67% for all lesions), ^{68}Ga-PSMA-11 PET/CT detected more lesions than mpMRI (13.5% versus 4.3% for index lesions, 18.2% versus 5.4% for all lesions, respectively) and lesions missed by mpMRI were significantly larger compared to lesions missed by ^{68}Ga-PSMA-11 PET/CT (1.66 cm^3 versus 0.72 cm^3). These findings led the authors to conclude that ^{68}Ga-PSMA-11 PET/CT offers improved index lesion and secondary cancer detection, as well as superior tumor localization compared to mpMRI. In another recent study, Spohn *et al.* [38] determined intraprostatic gross tumor volume (GTV) in 101 patients who underwent mpMRI and ^{68}Ga-PSMA-11 PET/CT prior to radical prostatectomy for biopsy-proven prostate cancer and determined ^{68}Ga-PSMA-11 PET/CT detected a significantly larger median GTV (4.9 mL versus 2.8 mL, respectively) and identified significantly more bilateral lesions (71 versus 57, respectively) compared to mpMRI. Additionally, Roberts *et al.* [39▪] recently reported that increasing intraprostatic PSMA intensity on preoperative ^{68}Ga-PSMA-11 PET/CT was significantly associated with higher Gleason score, presence of positive surgical margin, and upgrading from biopsy on final pathology. Most notably, PSMA intensity was significantly higher for patients with GG3 or higher disease compared to those with GG2 or lower disease on final pathology (SUV_{max} 10.37 versus 6.6). Moreover, for patients with GG2 prostate cancer on biopsy, PSMA intensity was the most significant predictor of progression-free survival following radical prostatectomy (HR 5.48 for $SUV_{max} > 8$ versus $SUV_{max} < 8$). Although these findings have the potential to substantially aid in prognostication for patients with GG2 prostate cancer considering active surveillance, focal therapy, or radical whole gland therapy as treatment options, further investigations are needed to validate these results.

Due to a longer half-life and lower positron energy, ^{18}F-labeled agents may produce PET/CT images of higher quality compared to those acquired using ^{68}Ga-labeled agents [40]. Gaur *et al.* [41▪] investigated both ^{18}F-DCFPyL PET/CT and mpMRI in 26 patients with high-risk, localized prostate cancer prior to targeted prostate biopsy and report similar sensitivities (^{18}F-DCFPyL 90.9% versus mpMRI 86.4%) and tumor detection rates (^{18}F-

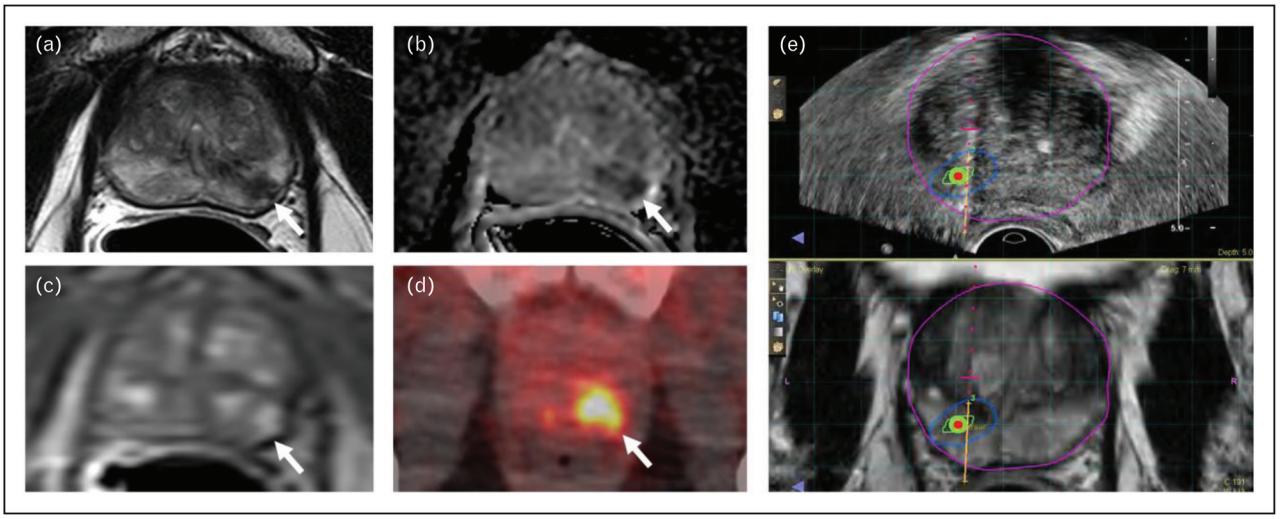

FIGURE 2. 73-year-old male with a serum PSA of 4.74ng/ml. Axial T2W MRI shows a heterogeneous hypointense lesion in the left apical-mid peripheral zone (arrow) (a), which shows diffusion restriction on ADC map (arrow) (b) and early enhancement on DCE MRI (arrow) (c). 18F-DCFPyL PET/CT demonstrates focal tracer uptake within the left apical-mid peripheral zone lesion (arrow) (d). TRUS/MRI fusion guided biopsy revealed Gleason 4+4 prostate cancer within this lesion (e). MRI, magnetic resonance imaging; TRUS, transrectal ultrasound.

DCFPyL 80% versus mpMRI 88.4%) for both imaging modalities (Fig. 2). Importantly, additional parameters obtained from ^{18}F-DCFPyL PET/CT, including total lesion PSMA and PSMA-derived tumor volume, were associated with increasing biopsy GG and PSMA intensity was significantly higher in malignant versus benign prostate tissue. In another recent study, Kuten *et al.* [42] compared ^{18}F-PSMA-1007 with ^{68}Ga-PSMA-11 PET/CT in 16 patients prior to radical prostatectomy. Interestingly, the authors report excellent concordance between ^{18}F-PSMA-1007 and ^{68}Ga-PSMA-11 for detecting intraprostatic lesions (κ: 0.871–1.0); however, in four cases ^{18}F-PSMA-1007 PET/CT identified unique secondary lesions that were histologically confirmed to be GG1 prostate cancer.

PSMA-targeted PET/MRI is a novel imaging modality that combines the excellent sensitivities and specificities for prostate cancer detection reported for PSMA-targeted radiotracers with the enhanced anatomical detail, soft tissue characterization, and spatial resolution afforded by MR imaging of the prostate [43]. Eiber *et al.* [44] analyzed mpMRI, PET, and ^{68}Ga-PSMA HBED-CC PET/MRI in 53 patients and compared the diagnostic capabilities of each imaging modality. Cancer was detected in 66%, 92%, and 98% of patients via mpMRI, PET, and PET/MRI, respectively, with PET and PET/MRI both significantly more sensitive in detecting prostate cancer than mpMRI. On an individual lesion level, mpMRI, PET, and PET/MRI demonstrated sensitivities of 58%, 64%, and 76%, and specificities of 82%, 94%, and 97%, respectively. Moreover, PET/MRI demonstrated a significantly higher AUC for localization of prostate cancer compared to mpMRI (0.88 versus 0.73) and PET (0.88 versus 0.83). More recently, Ferraro *et al.* [45] performed ^{68}Ga-PSMA-11 PET/MRI-guided targeted prostate biopsy on 42 patients and report a sensitivity of 96%, specificity of 81%, NPV of 93%, positive predictive value (PPV) of 89%, and accuracy of 90% for the detection of csPCa at the patient-level (defined as ISUP GG3 and/or cancer core length $\geq$ 6 mm). Overall, PSMA-targeted PET/MRI represents a highly accurate imaging modality to localize csPCa and may have the potential to further optimize image-guided diagnostic and therapeutic procedures. Further studies are needed to validate these findings and define the clinical utility of PSMA-targeted PET/MRI in the setting of focal therapy.

ULTRASOUND

Systematic TRUS-guided biopsy has historically served as the primary means for the diagnosis of prostate cancer. Despite its accessibility and cost-efficiency, TRUS-guided biopsy is associated with poor sensitivity and specificity for prostate cancer detection [1]. Several novel US imaging modalities have recently been reported with the objective of maintaining the benefits of US-based imaging while optimizing the diagnosis of csPCa. Contrast-enhanced US (CEUS) involves administration of an intravenous ultrasound-enhancing agent, such as microbubbles of air or lipid, prior to performing high-resolution US to visualize the microvascular architecture and evaluate tissue perfusion of a region of interest in real-time [46]. de Castro Abreu *et al.* [47] produced one of the first reports of CEUS to

monitor patients at 6 and 12 months following HIFU hemiablation for prostate cancer. More recently, Apfelbeck *et al.* [48] performed CEUS of planned treatment zones prior to, immediately after, and at 24 h after HIFU hemi- or whole-gland ablation and reported a decrease in visualized microbubbles, indicative of reduced microcirculation, in the ablated area. The same group later reported their experience using CEUS at 3, 6, 9, and 12 months following HIFU hemi- or whole-gland ablation and observed no evidence of microvascularization or perfusion within the treated area in any of the images obtained during follow-up [49]. Of note, the authors utilized CEUS/MRI fusion imaging to ensure consistent monitoring of treatment zones. Perioperative use of CEUS has also been evaluated in patients undergoing irreversible electroporation with a similar documented reduction in tumor microcirculation following treatment and favorable diagnostic accuracy compared to MRI (sensitivity 76%, specificity 81%, PPV 73%, and NPV 83%) [50]. Additionally, Bacchetta *et al.* [51▪▪] performed focal HIFU ablation on 32 patients with MR-visible, biopsy-confirmed prostate cancer with intraoperative CEUS at the conclusion of the procedure; if the initial ablation was deemed inadequate, a second focal HIFU ablation followed by repeat CEUS was performed. Using posttreatment in-field biopsies as the gold standard, CEUS demonstrated a sensitivity of 40%, specificity of 65%, PPV of 33%, and NPV of 71% for the detection of residual csPCa (GG2 or higher and/or maximum cancer core length $\geq$ 4 mm). Intraoperative CEUS images were then compared to mpMRI obtained 5 to 10 days after treatment with an agreement rate of 72.7% (κ: 0.45). CEUS appears to be a promising technology with capabilities to assess the adequacy of ablation of planned treatment zones in real-time. Further evaluation of CEUS in a larger, more diverse patient population using a variety of focal therapy modalities and treatment templates is necessary to validate this technology.

The ExactVu 29 MHz Micro-Ultrasound (MUS) System (Exact Imaging, Ontario, Canada) is a novel imaging modality that generates high-resolution (70 microns) images displaying detailed views of prostate anatomy for improved visualization of intraprostatic lesions in real-time [52▪]. To better characterize the underlying risk of csPCa in lesions identified on microUS, the Prostate Risk Identification using MUS (PRI-MUS) grading system was described and validated in 2016 [53]. Multiple studies have since been performed comparing the diagnostic accuracy of microUS to mpMRI. A recent multicenter, prospective study from Klotz *et al.* [54] enrolled 1040 patients who underwent microUS-targeted biopsy (for PRI-MUS $>$ 3 lesions) and mpMRI-targeted biopsy (for PI-RADS $>$ 3 lesions) followed by systematic biopsy. Compared to mpMRI, microUS demonstrated higher sensitivity (94% versus 90%) and NPV (85% versus 77%) with similar specificity (both 22%) and PPV (44% versus 43%) for the detection of csPCa (GG $\geq$ 2). Sountoulides *et al.* [55▪] performed a systematic review and meta-analysis of studies comparing the diagnostic accuracy of microUS-targeted biopsy to mpMRI-targeted biopsy and report a similar prostate cancer detection rate across all grades (overall detection rate, as well as rates for clinically significant and insignificant disease) for both imaging modalities. The detection ratio for GG1 disease was 0.94 (95% CI 0.73–1.22, $I^2 = 0$) compared to 1.05 (95% CI 0.93–1.19, $I^2 = 0$) for GG $\geq$ 2 disease, whereas the overall detection ratio for prostate cancer was 0.99 (95% CI 0.89–1.11, $I^2 = 0$). Of note, recent studies have reported the benefit of adding microUS-targeted lesions to mpMRI-targeted lesions and systematic biopsy. Rodriguez Socarras *et al.* [56] report the addition of microUS-targeted biopsy uniquely identified 11% of all diagnosed prostate cancers and all but one of these cases represented csPCa. In a similar fashion, Lughezzani *et al.* [57] demonstrate the addition of microUS-targeted lesions uniquely diagnosed 2.6% of csPCa in their cohort. Given the benefit demonstrated by adding microUS-targeted biopsy, combining this novel imaging modality with mpMRI may serve to further optimize the detection of csPCa. Further studies are warranted to determine the role of microUS, alone or in combination with mpMRI, to characterize intraprostatic lesions for diagnostic and therapeutic procedures.

CONCLUSION

Each of these novel imaging modalities has emerged as promising tools to enhance the focal therapist's ability to not only better localize and define the boundaries of intraprostatic lesions for treatment planning, but to also more accurately determine the adequacy of ablation intraoperatively and in posttreatment follow-up. In overcoming many of the limitations associated with contemporary mpMRI, the continued validation of these imaging modalities in diverse patient populations using a variety of focal therapy modalities and treatment templates will be essential for prostate cancer focal therapy to realize its potential.

Acknowledgements

None.

Financial support and sponsorship

This work was in part made possible through the NIH Medical Research Scholars Program, a public-private

partnership supported jointly by the NIH and contributions to the Foundation for the NIH from the Doris Duke Charitable Foundation, the American Association for Dental Research, the Colgate-Palmolive Company, and other private donors. NIH and Philips have a Cooperative Research and Development Agreement. NIH has intellectual property in the field, including among other patents and patent applications, Patent: 'System, methods, and instrumentation for image-guided prostate treatment' US Patent number: 8948845, with inventors/authors and P.A.P. NIH and Philips (InVivo Inc) have a licensing agreement. NIH and author P.A.P. receive royalties for a licensing agreement with Philips/InVivo Inc. NIH does not endorse or recommend any commercial products, processes, or services. The views and personal opinions of authors expressed herein do not necessarily reflect those of the US Government, nor reflect any official recommendation nor opinion of the NIH nor National Cancer Institute.

Conflicts of interest

There are no conflicts of interest.

REFERENCES AND RECOMMENDED READING

Papers of particular interest, published within the annual period of review, have been highlighted as:

- ■ of special interest
- ■■ of outstanding interest

1. Loeb S, Bjurlin MA, Nicholson J, *et al.* Overdiagnosis and overtreatment of prostate cancer. Eur Urol 2014; 65:1046–1055.
2. Ahmed HU, E-SBA. Brown LC, *et al.* Diagnostic accuracy of multiparametric MRI and TRUS biopsy in prostate cancer (PROMIS): a paired validating confirmatory study. Lancet 2017; 389:815–822.
3. Drost FJH, Osses DF, Nieboer D, *et al.* Prostate MRI, with or without MRI-targeted biopsy, and systematic biopsy for detecting prostate cancer. Cochrane Database Syst Rev 2019; 4: CD012663.
4. Klotz L, Chin J, Black PC, *et al.* Comparison of multiparametric magnetic resonance imaging–targeted biopsy with systematic transrectal ultrasonography biopsy for biopsy-naive men at risk for prostate cancer: a phase 3 randomized clinical trial. JAMA Oncol 2021; 7:534–542.
5. Rouvière O, Puech P, Renard-Penna R, *et al.* Use of prostate systematic and targeted biopsy on the basis of multiparametric MRI in biopsy-naive patients (MRI-FIRST): a prospective, multicentre, paired diagnostic study. Lancet Oncol 2019; 20:100–109.
6. Veeru Kasivisvanathan MRCS, Antti S, Rannikko PhD, *et al.* for the PRECISION Study Group Collaborators. MRI-targeted or standard biopsy for prostate-cancer diagnosis. N Engl J Med 2018; 378:1767–1777.
7. Ahdoot M, Wilbur AR, Reese SE, *et al.* MRI-targeted, systematic, and combined biopsy for prostate cancer diagnosis. N Engl J Med 2020; 382:917–928.
8. Siddiqui MM, Rais-Bahrami S, Turkbey B, *et al.* Comparison of MR/ultrasound fusion–guided biopsy with ultrasound-guided biopsy for the diagnosis of prostate cancer. JAMA 2015; 313:390–397.
9. Turkbey B, Mani H, Shah V, *et al.* Multiparametric 3T prostate magnetic resonance imaging to detect cancer: histopathological correlation using prostatectomy specimens processed in customized magnetic resonance imaging based molds. J Urol 2011; 186:1818–1824.
10. Borofsky S, George AK, Gaur S, *et al.* What are we missing? False-negative cancers at multiparametric MR imaging of the prostate. Radiology 2018; 286:186–195.
11. Filson CP, Natarajan S, Margolis DJ, *et al.* Prostate cancer detection with magnetic resonance-ultrasound fusion biopsy: the role of systematic and targeted biopsies. Cancer 2016; 122:884–892.
12. ■ Sathianathen NJ, Omer A, Harriss E, *et al.* Negative predictive value of multiparametric magnetic resonance imaging in the detection of clinically significant prostate cancer in the prostate imaging reporting and data system era: a systematic review and meta-analysis. Eur Urol 2020; 78:402–414.

Recent systematic review and meta-analysis reporting on the negative predictive value of mpMRI for clinically significant prostate cancer.

13. Wysock JS, Mendhiratta N, Zattoni F, *et al.* Predictive value of negative 3T multiparametric magnetic resonance imaging of the prostate on 12-core biopsy results. BJU Int 2016; 118:515–520.
14. Priester A, Natarajan S, Khoshnoodi P, *et al.* Magnetic resonance imaging underestimation of prostate cancer geometry: use of patient specific molds to correlate images with whole mount pathology. J Urol 2017; 197:320–326.
15. Merrick GS, Gutman S, Andreini H, *et al.* Prostate cancer distribution in patients diagnosed by transperineal template-guided saturation biopsy. Eur Urol 2007; 52:715–724.
16. Steensma BR, Luttje M, Voogt IJ, *et al.* Comparing signal-to-noise ratio for prostate imaging at 7T and 3T. J Magn Reson Imaging 2019; 49:1446–1455.
17. Laader A, Beiderwellen K, Kraff O, *et al.* 1.5 versus 3 versus 7 Tesla in abdominal MRI: a comparative study. PLoS One 2017; 12:e0187528.
18. Maas MC, Vos EK, Lagemaat MW, *et al.* Feasibility of T2-weighted turbo spin echo imaging of the human prostate at 7 tesla. Magn Reson Med 2014; 71:1711–1719.
19. Durand M, Jain M, Robinson B, *et al.* Magnetic resonance microscopy may enable distinction between normal histomorphological features and prostate cancer in the resected prostate gland. BJU Int 2017; 119:414–423.
20. Heidkamp J, Hoogenboom M, Kovacs IE, *et al.* Ex vivo MRI evaluation of prostate cancer: localization and margin status prediction of prostate cancer in fresh radical prostatectomy specimens. J Magn Reson Imaging 2018; 47:439–448.
21. Esteva A, Robicquet A, Ramsundar B, *et al.* A guide to DL in healthcare. Nat Med 2019; 25:24–29.
22. Castillo T JM, Arif M, Niessen WJ, *et al.* Automated classification of significant prostate cancer on MRI: a systematic review on the performance of machine learning applications. Cancers 2020; 12:1606.
23. Montagnon E, Cerny M, Cadrin-Chenevert A, *et al.* Deep learning workflow in radiology: a primer. Insights Imaging 2020; 11:22.
24. ■ Turkbey B, Haider MA. Deep learning-based artificial intelligence applications in prostate MRI: brief summary. Br J Radiol 2021; 94:20210563.

Comprehensive review of artificial intelligence and deep learning concepts in prostate MRI.

25. Arif M, Schoots IG, Tovar JC, *et al.* Clinically significant prostate cancer detection and segmentation in low-risk patients using a convolutional neural network on multiparametric MRI. Eur Radiol 2020; 30:6582–6592.
26. Gaur S, Lay N, Harmon SA, *et al.* Can computer-aided diagnosis assist in the identification of prostate cancer on prostate MRI? a multicenter, multireader investigation. Oncotarget 2018; 9:33804–33817.
27. Schelb P, Kohl S, Radtke JP, *et al.* Classification of cancer at prostate MRI: deep learning versus clinical PI-RADS assessment. Radiology 2019; 293:607–617.
28. Song Y, Zhang YD, Yan X, *et al.* Computer-aided diagnosis of prostate cancer using a deep convolutional neural network from multiparametric MRI. J Magn Reson Imaging 2018; 48:1570–1577.
29. Yoo S, Gujrathi I, Haider MA, Khalvati F. Prostate cancer detection using deep convolutional neural networks. Sci Rep 2019; 9:1–10.
30. Zhong X, Cao R, Shakeri S, *et al.* Deep transfer learning-based prostate cancer classification using 3 Tesla multiparametric MRI. Abdom Radiol 2019; 44:2030–2039.
31. Fraum TJ, Ludwig DR, Kim EH, *et al.* Prostate cancer PET tracers: essentials for the urologist. Can J Urol 2018; 25:9371–9383.
32. Wright GL, Haley C, Beckett ML, *et al.* Expression of prostate-specific membrane antigen in normal, benign, and malignant prostate tissues. Urologic Oncology: Seminars and Original Investigations 1995; 1:18–28.
33. Farolfi A, Ceci F, Castellucci P, *et al.* 68 Ga-PSMA-11 PET/CT in prostate cancer patients with biochemical recurrence after radical prostatectomy and PSA< 0.5 ng/ml. Efficacy and impact on treatment strategy. Eur J Nucl Med Mol Imaging 2019; 46:11–19.
34. Giesel FL, Knorr K, Spohn F, *et al.* Detection efficacy of 18F-PSMA-1007 PET/CT in 251 patients with biochemical recurrence of prostate cancer after radical prostatectomy. J Nucl Med 2019; 60:362–368.
35. Hofman MS, Lawrentschuk N, Francis RJ, *et al.* Prostate-specific membrane antigen PET-CT in patients with high-risk prostate cancer before curative-intent surgery or radiotherapy (proPSMA): a prospective, randomised, multicentre study. Lancet 2020; 395:1208–1216.
36. Morris MJ, Rowe SP, Gorin MA, *et al.* Diagnostic performance of 18F-DCFPyL-PET/CT in men with biochemically recurrent prostate cancer: results from the CONDOR Phase III, Multicenter Study. Clin Cancer Res 2021; 27:3674–3682.
37. Donato P, Morton A, Yaxley J, *et al.* 68 Ga-PSMA PET/CT better characterises localised prostate cancer after MRI and transperineal prostate biopsy: Is 68 Ga-PSMA PET/CT guided biopsy the future? Eur J Nucl Med Mol Imaging 2020; 47:1843–1851.
38. Spohn S, Jaegle C, Fassbender TF, *et al.* Intraindividual comparison between 68 Ga-PSMA-PET/CT and mpMRI for intraprostatic tumor delineation in patients with primary prostate cancer: a retrospective analysis in 101 patients. Eur J Nucl Med Mol Imaging 2020; 47:2796–2803.
39. ■ Roberts MJ, Morton A, Donato P, *et al.* 68 Ga-PSMA PET/CT tumour intensity preoperatively predicts adverse pathological outcomes and progression-free survival in localised prostate cancer. Eur J Nucl Med Mol Imaging 2021; 48:477–482.

Recent study demonstrating intraprostatic PSMA intensity on preoperative 68Ga-PSMA-11 PET/CT was significantly associated with adverse pathology and, in patients with GG2 disease, predicted progression-free survival following radical prostatectomy.

40. Werner RA, Derlin T, Lapa C, *et al.* 18F-labeled, PSMA-targeted radiotracers: leveraging the advantages of radiofluorination for prostate cancer molecular imaging. Theranostics 2020; 10:1–16.

41. ■ Gaur S, Mena E, Harmon SA, *et al.* Prospective evaluation of 18F-DCFPyL PET/CT in detection of high-risk localized prostate cancer: comparison with mpMRI. Am J Roentgenol 2020; 215:652–659.

Recent investigation demonstrating the utility of 18F-DCFPyL PET/CT for the detection of high-risk intraprostatic lesions.

42. Kuten J, Fahoum I, Savin Z, *et al.* Head-to-head comparison of 68Ga-PSMA-11 with 18F-PSMA-1007 PET/CT in staging prostate cancer using histopathology and immunohistochemical analysis as a reference standard. J Nucl Med 2020; 61:527–532.

43. Manfredi C, Fernández-Pascual E, Linares-Espinós E, *et al.* New frontiers in focal therapy for prostate cancer: prostate-specific membrane antigen positron emission tomography/magnetic resonance imaging. World J Clin Oncol 2021; 12:61–68.

44. Eiber M, Weirich G, Holzapfel K, *et al.* Simultaneous 68Ga-PSMA HBED-CC PET/MRI improves the localization of primary prostate cancer. Eur Urology 2016; 70:829–836.

45. Ferraro DA, Becker AS, Kranzbühler B, *et al.* Diagnostic performance of 68 Ga-PSMA-11 PET/MRI-guided biopsy in patients with suspected prostate cancer: a prospective single-center study. Eur J Nucl Med Mol Imaging 2021; 48:3315–3324.

46. Ashrafi AN, Nassiri N, Gill IS, *et al.* Contrast-enhanced transrectal ultrasound in focal therapy for prostate cancer. Curr Urol Rep 2018; 19:1–10.

47. de Castro Abreu AL, Ashrafi AN, Gill IS, *et al.* Contrast-enhanced transrectal ultrasound for follow-up after focal HIFU ablation for prostate cancer. J Ultrasound Med 2019; 38:811–819.

48. Apfelbeck M, Clevert D-A, Ricke J, *et al.* Contrast enhanced ultrasound (CEUS) with MRI image fusion for monitoring focal therapy of prostate cancer with high intensity focused ultrasound (HIFU). Clin Hemorheol Microcirc 2018; 69:93–100.

49. Apfelbeck M, Chaloupka M, Schlenker B, *et al.* Follow-up after focal therapy of the prostate with high intensity focused ultrasound (HIFU) using contrast enhanced ultrasound (CEUS) in combination with MRI image fusion. Clin Hemorheol Microcirc 2019; 73:135–143.

50. Jung EM, Engel M, Wiggermann P, *et al.* Contrast enhanced ultrasound (CEUS) with parametric imaging after irreversible electroporation (IRE) of the prostate to assess the success of prostate cancer treatment. Clin Hemorheol Microcirc 2021; 77:303–310.

51. ■■ Bacchetta F, Martins M, Regusci S, *et al.* The utility of intraoperative contrast-enhanced ultrasound in detecting residual disease after focal HIFU for localized prostate cancer. Urologic Oncology: Seminars and Original Investigations 2020; 38:846.e1–846.e7.

Recent report describing intraoperative postablation contrast-enhanced US to determine the adequacy of focal therapy to planned treatment zones and allow for immediate re-treatment.

52. ■ Dias AB, O'Brien C, Correas J-M, Ghai S. Multiparametric ultrasound and micro-ultrasound in prostate cancer: a comprehensive review. Br J Radiol 2021; 94:20210633.

Excellent review of multiparametric, including contrast-enhanced, ultrasound and micro-ultrasound imaging for prostate cancer.

53. Ghai S, Eure G, Fradet V, *et al.* Assessing cancer risk on novel 29 MHz micro-ultrasound images of the prostate: creation of the micro-ultrasound protocol for prostate risk identification. J Urol 2016; 196:562–569.

54. Klotz L, Lughezzani G, Maffei D, *et al.* Comparison of micro-ultrasound and multiparametric magnetic resonance imaging for prostate cancer: a multicenter, prospective analysis. Can Urol Assoc J 2021; 15:E11.

55. ■ Sountoulides P, Pyrgidis N, Polyzos SA, *et al.* Micro-ultrasound–guided vs multiparametric magnetic resonance imaging-targeted biopsy in the detection of prostate cancer: a systematic review and meta-analysis. J Urol 2021; 205:1254–1262.

Recent systematic review and meta-analysis demonstrating comparable cancer detection rates for microUS-guided and mpMRI-guided prostate biopsy.

56. Rodríguez Socarrás ME, Gomez Rivas J, Cuadros Rivera V, *et al.* Prostate mapping for cancer diagnosis: the Madrid Protocol. Transperineal prostate biopsies using multiparametric magnetic resonance imaging fusion and micro-ultrasound guided biopsies. J Urol 2020; 204:726–733.

57. Lughezzani G, Maffei D, Saita A, *et al.* Diagnostic accuracy of microultrasound in patients with a suspicion of prostate cancer at magnetic resonance imaging: a single-institutional prospective study. Eur Urol Focus 2021; 7:1019–1026.